


Thermo-oxidative crosslinking of carbon fiber reinforced PEEK (Polyetheretherketone) for additive manufactured ceramic matrix composites

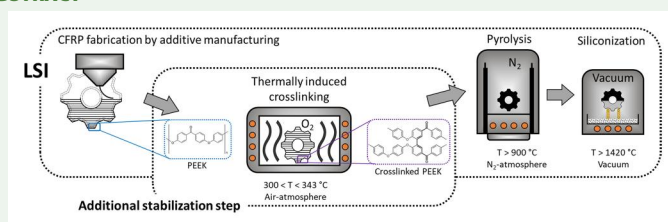
Wolfgang Freudenberg^a , Felix Wich^a, Jalena Best^a, Elena Moukhina^b, Tim Scherzer^c, Holger Ruckdäschel^c, Nico Langhof^a and Stefan Schafföner^a

^aChair of Ceramic Materials Engineering (CME), University of Bayreuth, Bayreuth, Germany; ^bNetzsch Gerätebau GmbH, Selb, Germany; ^cDepartment of Polymer Engineering, University of Bayreuth, Bayreuth, Germany

ABSTRACT

Carbon fiber reinforced polyetheretherketone (CF-PEEK) samples were fabricated using material extrusion. These additive manufactured green bodies are later processed to their final application as ceramic matrix composites (CMC) by the liquid silicon infiltration (LSI) route. Past studies showed that the application of material extrusion for the fabrication of CMC requires an additional stabilization-step after 3D-printing in order to prevent the remelting of CF-PEEK during the high temperature process of pyrolysis. The thermally induced crosslinking of the CF-PEEK parts ensured shape accuracy and avoided remelting during the pyrolysis afterwards but is limited by the melting temperature of PEEK ($T_m \sim 343^\circ\text{C}$). The study revealed a correlation between the annealing conditions time and temperature and the degree of crosslinking. Based on the analytical results from differential scanning calorimetry (DSC), a kinetic model was calculated, allowing predictions in dependence of the annealing temperature and time. Rheological and shape stability investigations of thermally annealed specimens verified the analytic results. The main findings of the study highlight an increasing degree of crosslinking with increasing annealing temperature and time.

GRAPHICAL ABSTRACT



ARTICLE HISTORY

Received 14 May 2024
Accepted 29 July 2024

KEYWORDS

Carbon fiber reinforced polyetheretherketone; material extrusion; thermal crosslinking; differential scanning calorimetry; kinetics

1. Introduction

Ceramic matrix composites (CMC) combine the advantages of monolithic ceramics, e.g. high specific strength and moduli, chemical resistance and high temperature stability, with the damage tolerance due to fiber reinforcement. They are therefore often applied for high-performance applications [1–7]. In many cases, carbon fibers are used due to their excellent mechanical and high temperature properties [3,8,9]. However, the high hardness and abrasion resistance make subtractive post-processing and the whole manufacturing of CMC exceedingly expensive [4]. Hence, new processes are necessary to reduce post-processing and associated costs. For this purpose, alternative green body manufacturing

techniques were introduced, e.g. additive manufacturing. Additive manufacturing combines the advantages of fabricating highly complex parts, reduces waste, load customized designs, easy scalability and tool-free fabrication [10–15]. Among the several additive manufacturing techniques, especially material extrusion technologies, fused filament fabrication (FFF) allows short and long fiber reinforcements. A schematic image of a part produced *via* FFF is illustrated in Figure 1. Many papers were published in the last years in this field, indicating the high potential of this technology [16–24].

Most of non-oxide CMC are manufactured by a multi-step process, starting with the green body fabrication of carbon fiber reinforced polymer (CFRP). Usually thermosets, especially phenolic based

CONTACT Wolfgang Freudenberg  wolfgang.freudenberg@uni-bayreuth.de  Chair of Ceramic Materials Engineering (CME), University of Bayreuth, Prof.-Rüdiger-Bormann-Str. 1, 95447 Bayreuth, Germany.

© 2024 The Author(s). Published by Informa UK Limited, trading as Taylor & Francis Group.

This is an Open Access article distributed under the terms of the Creative Commons Attribution License (<http://creativecommons.org/licenses/by/4.0/>), which permits unrestricted use, distribution, and reproduction in any medium, provided the original work is properly cited. The terms on which this article has been published allow the posting of the Accepted Manuscript in a repository by the author(s) or with their consent.

powders and liquids/fluids, are used [25]. During the shaping process, the polymeric thermoset undergoes irreversible covalent crosslinking, rendering it non-meltable and conferring a stable shape. However, during the last years, the use of thermoplastic-based matrices for CMC applications increased [26–32].

In order to finally manufacture a CMC based on additively manufactured CFRP, the CFRP will be first pyrolyzed and then converted by liquid silicon infiltration (LSI) to obtain the final C/C-SiC part. This process requires the use of polymeric matrix precursors with a carbon yield after pyrolysis (1000 °C, nitrogen) of at least 30 wt.%, which drastically limits the number of potential thermoplastic candidate materials. Previous investigations identified polyetheretherketone (PEEK) as well as carbon fiber reinforced PEEK (CF-PEEK) as suitable [26–30], due to the high carbon yield of PEEK after pyrolysis in nitrogen of about 40–50 wt.% [34–37]. Furthermore, PEEK is employed in numerous medical applications, including tissue engineering, and is a well-established material for additive manufacturing processes [38–44]. However, most studies focused primarily on topics like biocompatibility, degradation, mechanical properties and processibility of additive-manufactured PEEK and derived composites.

The challenge of using PEEK and other thermoplastics for the LSI process is the reversible melting behavior. Consequently, it is necessary to stabilize the thermoplastics before the pyrolysis to avoid remelting and to obtain shape accuracy. Figure 2 demonstrates

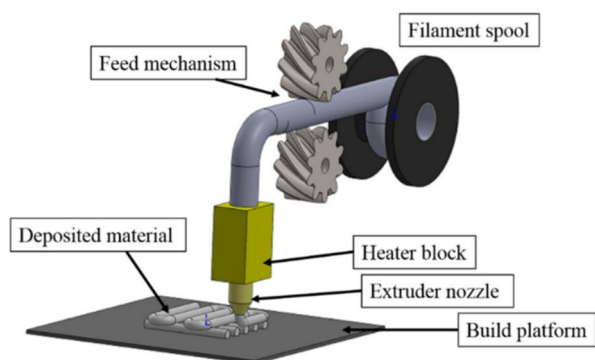


Figure 1. Schematic of the fused filament fabrication [33].

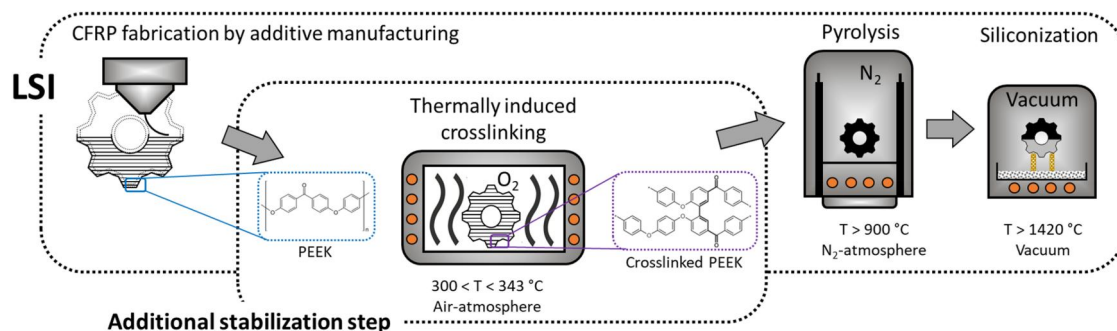


Figure 2. Schematic LSI process combined with the additional stabilization step and the typical process conditions.

the schematic LSI process, including the process conditions and the additional stabilization step realized by thermally induced crosslinking. This additional stabilization step is the main focus of this study.

Previously, two methods of crosslinking PEEK were reported [45]. The first method was thermally induced crosslinking at 400 °C, and the second method was proton-beam crosslinking. Thermo-oxidative ageing of PEEK was explained by the formation of radicals, leading to crosslinking [46]. During the last years, many publications investigated the influence of thermal treatments on PEEK and CF-PEEK, respectively, but most of them dealt with temperatures above the melting temperature of PEEK [46–51]. Nevertheless, in order to further process additively manufactured complex CFRP parts, the thermal crosslinking must be carried out below the melting temperature of PEEK ($T_m \sim 343$ °C) to maintain shape accuracy. On the other hand, the temperature must be high enough to initiate a crosslinking effect of the CF-PEEK. Figure 3 illustrates a schematic process window as a function of the crosslinking.

The main aim of this study is therefore to determine the influence of the final thermal annealing temperature in combination with a variation of annealing time on the shape stability for the following LSI process to complete the conversion of additively manufactured parts to a CMC. Thus, the results of the investigated methods determine the crosslinking effects of PEEK as a function of the thermal annealing parameters. Additionally, the used analytic methods allowed to generate a kinetic model predicting the relation of crosslinking due to the thermal annealing temperature and time. Regarding the final processed part, the target was to avoid remelting in combination with the shape accuracy of the PEEK-based CFRP in order to fully benefit from the advantages of additive manufacturing.

2. Materials and methods

2.1. CFRP manufacturing

A commercial carbon fiber reinforced PEEK (CF-PEEK) filament (Desktop Metal[®]) with a density of 1.39 g/cm³, a diameter of 1.75 mm and a fiber

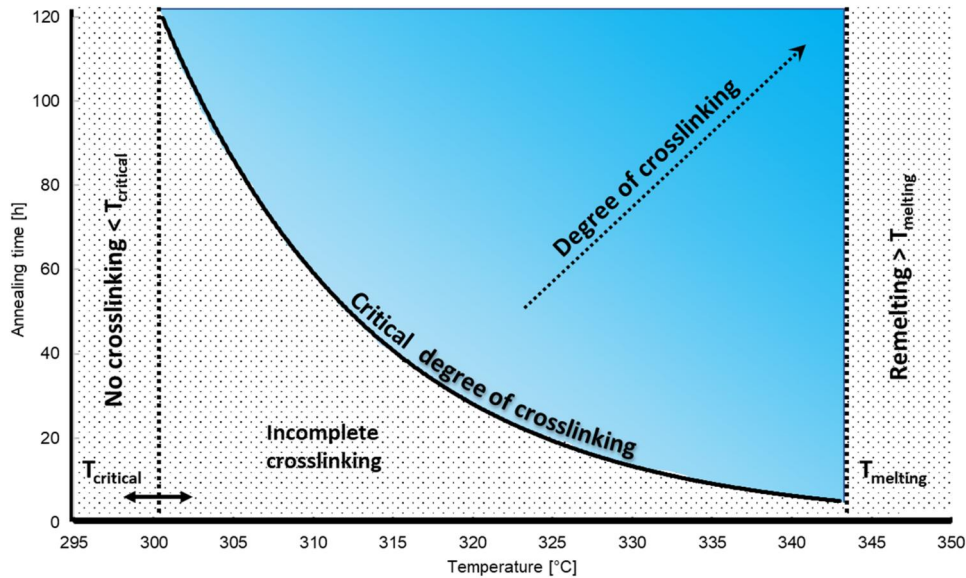


Figure 3. Schematic process window within the thermal limitations.

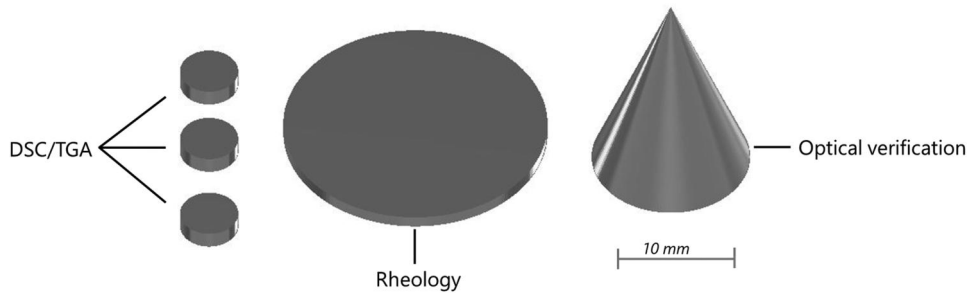


Figure 4. Sample geometries for the DSC/TGA and rheological analysis and the optical verification.

volume content of 13% was used for the CFRP manufacturing by FFF. The additively manufactured specimens were printed with an FFF printer (Funmat HT Enhanced, Intamsys, China). Each sample had a single layer height of $150\ \mu\text{m}$ and 80% infill. The printing direction was $\pm 45^\circ$, without any bottom and top layer, respectively. The printing speed was $25\ \text{mm}/\text{min}$, and the nozzle temperature was set to 410°C . Figure 4 shows the different sample geometries for the analytical methods. The DSC/TGA samples had a diameter of $5.5\ \text{mm}$ and a height of $1.7\ \text{mm}$, appropriate to the used crucibles. The weight of the samples was in the range of about $34\text{--}36\ \text{mg}$. The printed discs for rheological measurements had a diameter of $25\ \text{mm}$ and a height of $1.2\ \text{mm}$. For optical verification and shape stability tests, cone-shaped samples with a diameter of $15\ \text{mm}$ and a height of $20\ \text{mm}$ were manufactured.

2.2. Thermal induced crosslinking

The thermally induced crosslinking was carried out after the additive manufacturing step using a small convection furnace, having a precise temperature control, with a low heating rate of $2\ \text{K}/\text{min}$ in air (NAT 15/65, Nabertherm, Germany). The final

temperature varied between 315°C , 320°C , 325°C , 330°C and 335°C , whereas the dwell time was changed from $6\ \text{h}$, $12\ \text{h}$, $24\ \text{h}$ to $48\ \text{h}$. Compared to other furnaces, the direct heat radiation of the heating elements was avoided due to the setup with the metallic interior lining of the furnace.

2.3. Differential scanning calorimetry (DSC)

The influence of the annealing temperature and duration on the degree of thermally induced crosslinking was investigated by DSC (STA 449 F3 Jupiter, Netzsch Gerätebau GmbH, Germany) measurements in nitrogen atmosphere, using $85\ \mu\text{l}$ aluminum crucibles for an improved heat transfer, according to the program illustrated in Figure 5. The sample geometries were chosen according to Figure 4. The thermally induced crosslinking partially reduced the remelting of the thermoplastic PEEK. Therefore, DSC was used to analyze the melting enthalpy (ΔH_m) and the glass transition temperature T_g . The T_g was determined at the turning point of the second heating curve. Ehrenstein et al. [52] reported that the first heating cycle reveals information about the thermal and mechanical history, often mentioned as processing or manufacturing information,

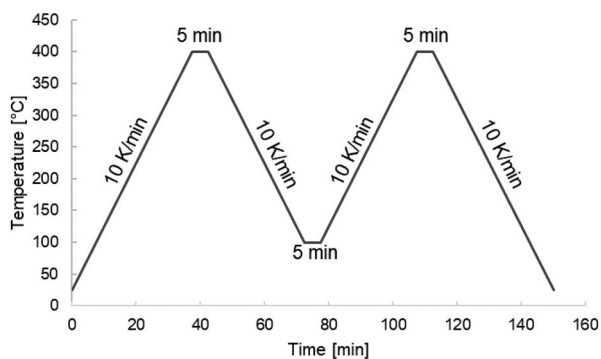


Figure 5. Schematic of the DSC cycle.

whereas the second cycle is used for the determination of material characteristics. Thus, for the final thermal analysis, the second heating step was essential for the analysis of the thermally induced crosslinking.

2.4. Kinetics

For the kinetic analysis of the thermal crosslinking, the melting enthalpy obtained after annealing was analyzed. The kinetic analysis was based on the data of the DSC measurements using a commercial software (Kinetics Neo, Version 2.6.7.8, Netzsch GmbH, Germany). The respective models are explained in section 3.2. The degree of conversion (D_C) was calculated as the ratio of the difference between the total melting enthalpy ($\Delta H_{m,total}$) and the residual melting enthalpy ($\Delta H_{m,residual}$) to the total melting enthalpy, shown in Equation (1).

$$D_C = \frac{\Delta H_{m,total} - \Delta H_{m,residual}}{\Delta H_{m,total}} \quad (1)$$

2.5. Rheology

The rheological measurements (MCR 702 Multidrive, Anton Paar, Germany) were performed to determine the storage and the loss modulus, respectively. The tests were carried out with an oscillating plate-plate geometry at a temperature of 400 °C in nitrogen atmosphere. The frequency was set to 10 Hz, and the amplitude sweep was performed in the range of 0.01–100%. The normal force was set to a value of 2 N.

2.6. Thermogravimetric analysis (TGA)

The final carbon yield, calculated as shown in Equation (2), was determined by thermogravimetric analysis (TGA) (STA 449 F3 Jupiter, Netzsch Holding, Germany) in nitrogen atmosphere up to 1050 °C and a heating rate of 10 K/min in accordance with the final temperature of the pyrolysis used in the LSI process. The $mass(T)$ is the mass of the

sample as a function of the temperature, in this case after 1050 °C.

$$Carbon\ yield = \frac{mass(T)}{initial\ mass} * 100\% \quad (2)$$

2.7. Sol-gel

To quantify the degree of crosslinking, the gel content of the thermally annealed samples was determined by extracting with concentrated sulfuric acid. Each sample (≈ 35 mg) was placed in 20 cm³ concentrated sulfuric acid at room temperature for 240 h under continuous stirring at low rates. Afterwards, the acid was decanted and the remaining gel was washed three times with distilled water. Finally, the samples were dried in a vacuum furnace at 75 °C for 24 h and the remaining gel mass was determined.

2.8. Shape stability

To verify the shape stability of the samples, the thermally annealed cone-shaped samples were compared. The specimens were first thermally annealed at the temperatures mentioned in section 2.2. Afterwards, they were heated up to 450 °C with a heating rate of 5 K/min and held at that temperature for one hour in a furnace with atmospheric air (NAT 15/65, Nabertherm, Germany). The softening and melting behavior of the pretreated parts were observed, and the heights were measured afterwards to quantify the effect of the thermal annealing.

3. Results and discussion

The effect of thermal treatments of PEEK and the occurring mechanism were explained in several previous studies [46,48–51,53,54]. It was described as a combination of oxidative chain scission reactions, chain branching reactions and crosslinking reactions, depending on the temperature, the duration and the atmosphere of the annealing. While the ageing and crosslinking of PEEK were much more affected in air atmosphere than in nitrogen.

In order to verify the hypothesis that the crosslinking degree of thermally annealed PEEK below the melting temperature is expected to increase with rising temperature and duration of the thermal annealing step, several analytical investigations were carried out.

Unless otherwise specified, the number of samples per parameter combination is one.

3.1. Differential scanning calorimetry (DSC)

Representative DSC curves are shown in Figure 6 for the as-printed sample and samples annealed at 335 °C. Figure 6 illustrates that increasing annealing times led to a gradual shift of the melting peak temperatures from 304 °C (as-printed) to 304 °C (annealed at 335 °C, 48 h).

The same tendency was observed for the melting enthalpy. Prolonged annealing times led to lower overall melting enthalpy values visible as reduced melting peak areas. Figure 7 presents the influence of annealing time and temperature on the melting enthalpy. The highest annealing temperature (335 °C) had the largest effect and steepest negative slope with a negligible melting enthalpy after 48 h. Moreover, it is obvious that the melting enthalpy decreased with increasing annealing time. The same effect was detected for the peak of the melting temperature of CF-PEEK in Figure 8.

Pascual et al. [46] reported the same effects for higher annealing temperatures above the melting point of PEEK at 400–450 °C and much shorter durations (30–300 s). The study showed that the crystallinity as well as the peak of melting temperature of PEEK decrease with degradation time and temperature. The same trend was also reported by Day et al. [50], and was confirmed for lower temperatures and expanded annealing times. Pascual et al. [46] explained that the decreasing crystallinity as well as the peak of melting temperature resulted from intermolecular branching of the original polymeric structure leading to crosslinking. The thermo-oxidative ageing of PEEK causes the formation of radical species close to ether bonds and keto groups, which then result in further reactions involving inter- and intramolecular processes [46]. These

chemical mechanisms cause crosslinking and intermolecular reactions, which were already well explained and summarized in previous studies in the melting state of PEEK [34,51,55]. Courvoisier et al. investigated PEEK in the rubber state in the temperature range of 180 °C–320 °C at different

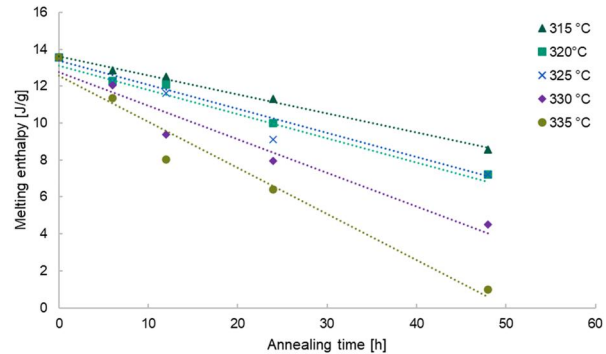


Figure 7. Melting enthalpy as a function of the annealing temperature and time with experimental points and linear approximation.

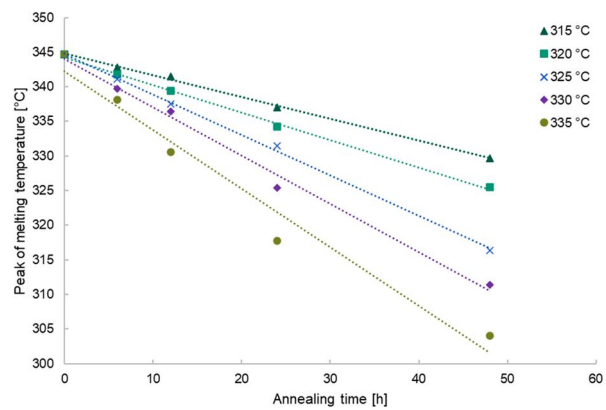


Figure 8. Peaks of melting temperature from DSC measurements as a function of the annealing temperature and time with experimental points and linear approximation.

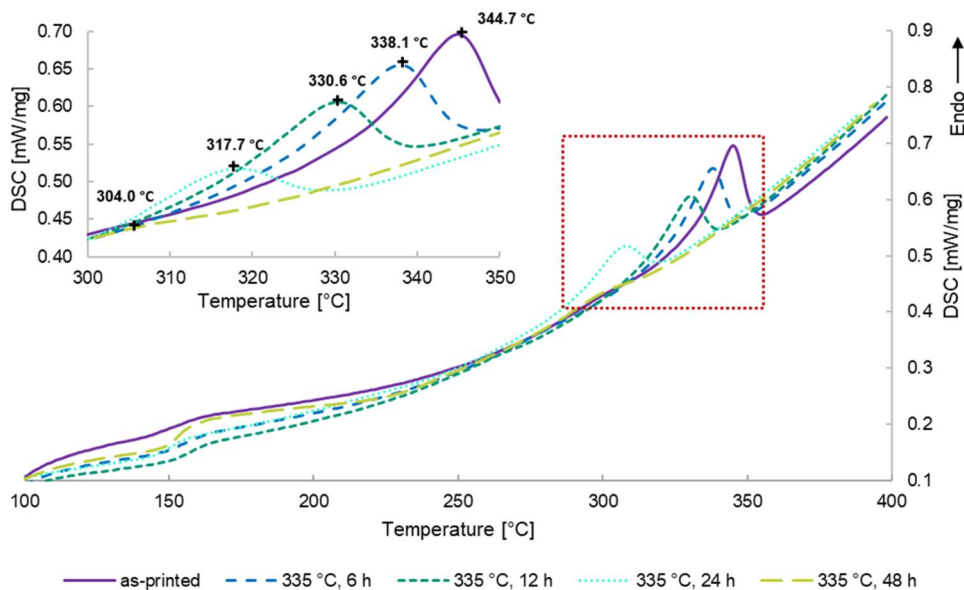


Figure 6. Representative DSC curves of the samples annealed at 335 °C during different annealing times and untreated “as-printed” sample.

oxygen partial pressures from 0.21 to 50 bars. They concluded that the oxidation of PEEK leads to a large predominance of crosslinking over chain scissions, resulting in a sharp increase of T_g , whereas the T_g decreases with the number of chain scissions. Moreover, the increased temperature accelerated the oxidation kinetics of PEEK. It was also explained that the thermal annealing formed an oxidized layer leading to reduced molecular mobility, thus preventing the annealing phenomenon of crystallization [56], resulting in a reduction of the melting enthalpy. In contrast to these studies, Zhang and Zeng [57] reported the opposing effect for the peak of melting temperature shift. They investigated the effect of thermal treatment of PEEK in the temperature range from 332 to 347 °C. PEEK powder was annealed for certain temperatures and annealing times in the range of 1–72 h in air. For annealing times of 4 h, they concluded that the melting point shifted to higher values for the samples annealed below the melting temperature, whereas the samples annealed above the melting temperature revealed two separate melting endotherms. The lower annealed samples (below the melting temperature) were not further considered in the study. In our study, the 2nd DSC heating curves were analyzed due to changes in the CF-PEEK samples and to extinguish the thermal history of the annealing process. Analyzing the 1st heating cycle (not shown here) like Zhang and Zeng did, the same results and trends were observed.

In comparison to these studies, the annealing temperatures in this study were consistently below the melting temperature to avoid remelting of the samples. The results for DSC data of annealed CF-PEEK listed in Table 1 indicate that there is a

Table 1. DSC results of annealed CF-PEEK.

Annealing temperature [°C]	Annealing time [h]	Melting enthalpy ΔH_m [J/g]	Melting temperature T_m [°C]	Glass transition temperature T_g [°C]
as-printed	–	13.56	344.7	154.5
315	6	12.87	342.8	154.2
	12	12.50	341.5	154.7
	24	11.32	337.0	155.8
	48	8.56	329.7	156.8
	6	12.28	341.8	154.8
320	12	12.09	339.4	153.7
	24	10.02	334.2	156.8
	48	7.22	325.5	159.2
	6	12.23	341.1	153.6
	12	11.63	337.5	154.3
325	24	9.12	331.5	156.0
	48	7.20	316.4	161.0
	6	12.05	339.7	154.3
	12	9.39	336.4	157.3
	24	7.95	325.4	158.2
330	48	4.50	311.4	163.0
	6	11.34	338.1	156.0
	12	8.02	330.6	157.5
	24	6.40	317.7	160.9
	48	1.00	304.0	158.6

critical lower limit of the temperature initializing a crosslinking effect. The temperatures investigated in this study were above this critical lower limit. However, a crosslinking effect at 319 °C with an annealing time of 24 h, postulating a thermally induced crosslinking for PEEK under certain conditions, was previously reported [58]. Based on the data of the current study and of Cebe [58,59], the lower temperature limit was assumed to be around 310 °C to initiate a crosslinking effect. Besides the temperature, the thermally induced crosslinking is also affected by the time. Below a critical annealing time <12 h, there was nearly no reduction of the melting enthalpy. Hence, a minimum annealing time is additionally required for the crosslinking reactions of PEEK.

Other studies have often described an increase in T_g as a result of crosslinking reactions [56]. In general, the glass transition temperature shown in Figure 9 increased with higher annealing temperature and time. Taking the present results into account, the hypothesis of the increasing degree of crosslinking with expanded annealing temperatures and times was confirmed.

However, the T_g of the 335 °C, 48 h sample was lower compared to the value of the 335 °C, 24 h sample. (To clearly show the main tendency of the T_g in Figure 9 the value of 335 °C, 48 h was not considered for the linear approximation.) It is assumed that the competing mechanism of chain scission and chain branching is dominated by the chain scission leading to shorter polymer chains and consequently to a lower degree of crosslinking. However, this is in contrast to the results of the melting enthalpy and the melting peak shift but could be a hint for an upper limitation of the thermal annealing process.

Moreover, as shown before in Figures 7 and 8, for low temperatures and a short annealing time of ≤ 12 h the T_g (Figure 9), as well as the melting enthalpy and the shift of melting peak were recognizable but weakened. Regarding the oxidation-

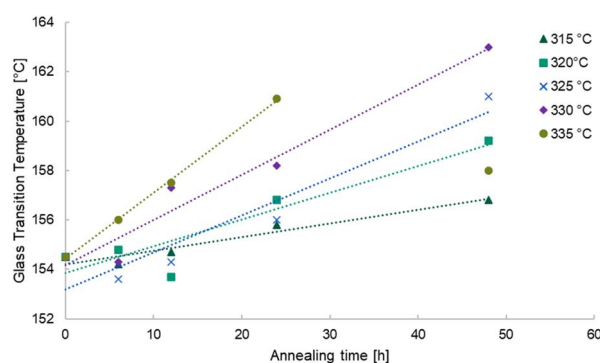


Figure 9. Glass transition temperature as a function of the annealing temperature and time with experimental points and linear approximation (except of 335 °C, 48 h).

based effects, it is evident that the influence of elevated annealing temperatures and extended times can be discerned.

3.2. Kinetic analysis

Almeida et al. [60] demonstrated qualitative predictions for factors influencing the degradation of CF-PEEK composites, based on rheological measurements. For solid state reactions, the degree of conversion α is normally used in kinetic analysis, which shows the relative fraction of the reacted material. Thus, for example, before the beginning of the reaction the value of conversion is zero, and after the end of the reaction the conversion is equal to one.

The kinetics of solid-state reactions is described by temperature dependence according to Arrhenius [61] with an activation energy E_a , as a differential equation (Equation 3).

$$\frac{d\alpha}{dt} = A * f(\alpha) * \exp\left(\frac{-E_a}{RT}\right) \quad (3)$$

where $f(\alpha)$ is a function of conversion α depending on the type of reaction, A is a pre-exponential factor, T is the absolute temperature in Kelvin, and R is the ideal gas constant with the value of 8.314 J/(mol*K).

These values present the enthalpy change during the isothermal measurements. The values decreased at the beginning faster, then slowly and finally asymptotically approaching their final value with zero melting enthalpy. This shape of the curves is characteristic of the n^{th} order reaction:

$$\frac{d\alpha}{dt} = A * (1 - \alpha)^n * \exp\left(\frac{-E_a}{RT}\right) \quad (4)$$

For the kinetic analysis of these experimental curves, the NETZSCH Kinetics Neo program was used with a model-based analysis for n^{th} order reaction. The experimental points were connected with the straight lines and interpolated points were calculated in order to have the curves with enough data points for the fit. As a result of the kinetic model, the optimal parameters A , E_a , and n in Equation (4) were found. The model well describes the measured experimental data for all measured temperatures.

Figure 10 shows the curves for the kinetic model of the n^{th} order reaction with the following parameters:

Based on the measured data and the kinetic analysis, a model for the prediction of the melting enthalpy in dependence of different temperatures and times was created. This model, shown in Figure 11, is in accordance with the data of Figure 10 and extended for longer times. This model allows predictions to be made for any temperature and time

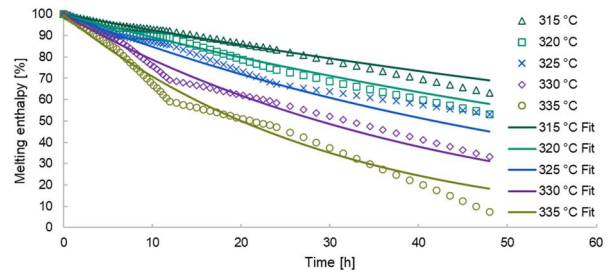


Figure 10. Experimental data for melting enthalpy with linear interpolation (dots) and kinetic model (solid lines) for n^{th} order reaction with optimal parameters for different annealing temperatures.

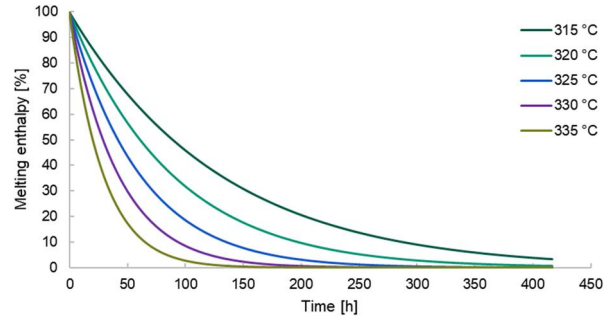


Figure 11. Prediction of residual melting enthalpy as a function of time for different temperatures.

but may lose accuracy for temperatures and times far outside the value range.

3.3. Rheology

Additional rheological tests were carried out to confirm the DSC results. The results are shown in Figure 12 for the samples annealed for 48 h. As illustrated in Figure 12, the storage modulus of the annealed samples was more than two magnitudes higher than that of the untreated sample. Furthermore, the higher the temperature at constant annealing times, the higher the storage modulus, except for the 335 °C, 48 h sample. This in turn is in agreement with the results of the glass transition temperature of this sample determined by DSC in Figure 9. Contrary to the previous results, the T_g and the storage modulus for these parameters decreased in comparison with the samples annealed at 330 °C for 48 h. The lower values can be explained by the competing mechanism that occurs during thermal treatments of PEEK close to its melting point. The reduced elastic response combined with the lower glass transition temperature of the samples annealed at 335 °C for 48 h is associated with the predominance of chain scission reactions over possible competing crosslinking effects. To further investigate the opposing effects of crosslinking and chain scission and the kinetics thereof, additional analytical methods such as CP/MAS NMR, FTIR or Raman spectroscopy may prove useful to

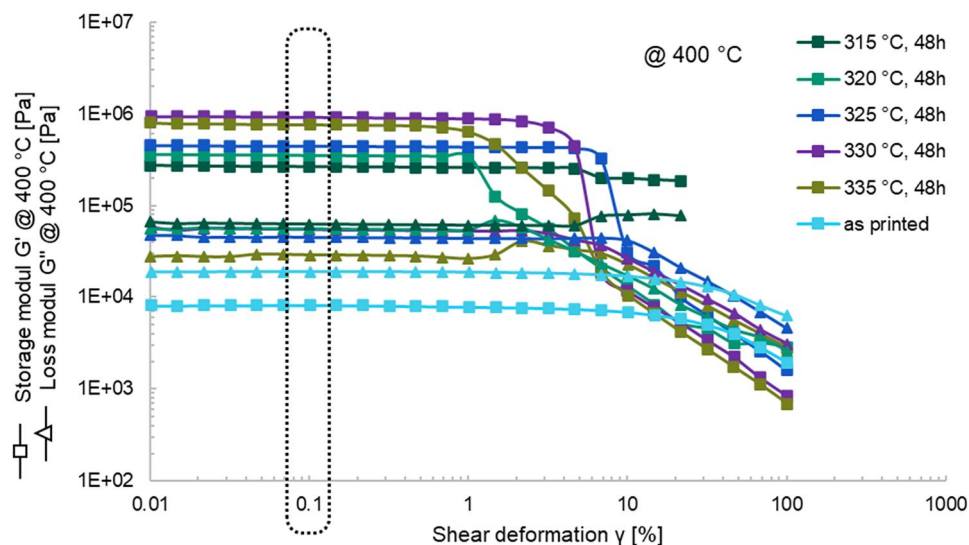


Figure 12. Storage and loss modulus as a function of shear deformation at 400 °C of the samples annealed for 48h.

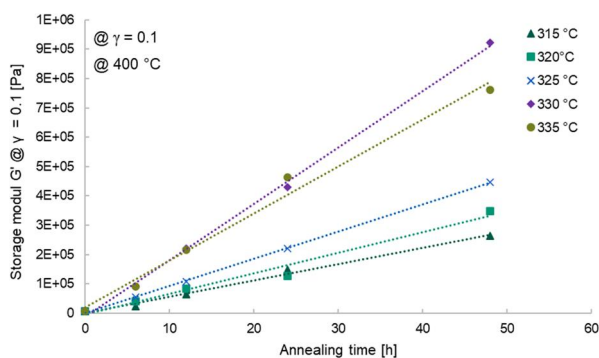


Figure 13. Storage modules at a shear rate of 0.1% and 400 °C as a function of annealing time.

investigate the resulting polymer structure in more detail in the following studies.

Compared to the untreated sample, the storage modules of the annealed samples showed higher values than the loss modules for each sample. Furthermore, the storage and loss modules diverge with increasing annealing temperature and time (not shown here). Thus, the elastic amount increases in the same way as the annealing temperature and time increase, indicating crosslinking effects, which led to higher network densities. The storage and loss modules showed an almost constant level up to a shear deformation of 1% before reaching the plastic deformation, dropping afterwards.

Therefore, to compare the storage modules for each annealed specimen, the values at a shear deformation of 0.1% are shown in Figure 13.

The DSC results were confirmed by the rheological tests. The storage modules were less affected at low annealing temperatures and times than at higher ones. This is also in good agreement with the post-test rheological specimens shown in Figure 14. The deformation and melting behavior were strongly influenced by the annealing conditions. The as-printed specimen and each of the 6 h annealed

specimens were (partially) melted and destroyed, whereas each of the 48 h annealed specimens was still in shape.

3.4. Thermogravimetric analysis (TGA)

It was shown for phenolic resins that the carbon yield after pyrolysis up to 1050 °C in nitrogen atmosphere increased with a higher degree of cross-linking [25]. However, the detailed results of the thermogravimetric analysis in Table 2 did not confirm this tendency for the CF-PEEK samples investigated in this study.

The curves of each sample are illustrated in Figure 15. The carbon yields of the samples were in the range of 59.2–61.2 wt.% and showed no clear tendency. Usually, the carbon yield correlates with the degree of crosslinking. The resulting network would be expected to have a similar effect on the carbon yield as shown by Wich et al. [25]. This might not always be the case – especially if the mechanism of PEEK degradation in this temperature region would not be crosslinking exclusively. The combination of scission and crosslinking leading to some amount of shorter polymeric chains (thus decreasing the total yield) as well as longer chains (results of crosslinking) counteract this relation.

3.5. Sol-gel tests

Additional to the thermal analysis by TG/DSC and DMA, the chemical resistance of PEEK samples against concentrated sulfuric acid was investigated. Annealed samples thereby showed increased resistance against the acid and only partly dissolved during the trials. Untreated samples, on the other hand, were dissolved completely. This further underlines the chemical changes during annealing of samples

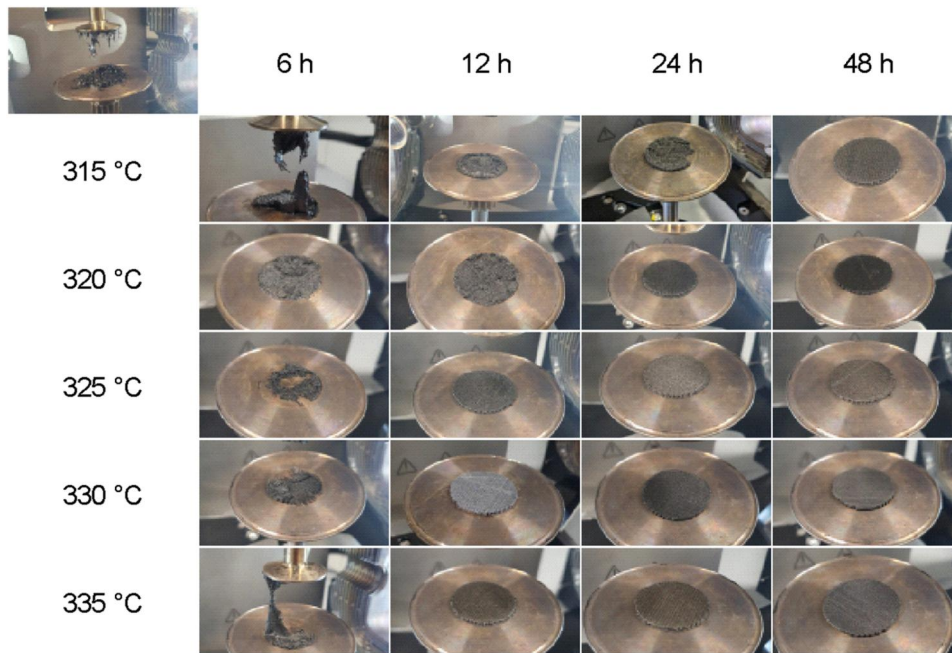


Figure 14. Specimens after the rheological tests at 400 °C.

Table 2. Residual mass measured by TGA up to 1000 °C in nitrogen, as a function of the annealing temperature and time.

	Thermal treatment [°C]	Annealing time [h]			
		6	12	24	48
	315	59.23	60.46	60.80	60.04
	320	60.06	60.69	60.67	60.60
	325	60.77	60.82	60.24	60.64
	330	61.00	60.88	60.30	60.65
	335	61.17	60.26	60.84	60.97

The as-printed (59.65%).

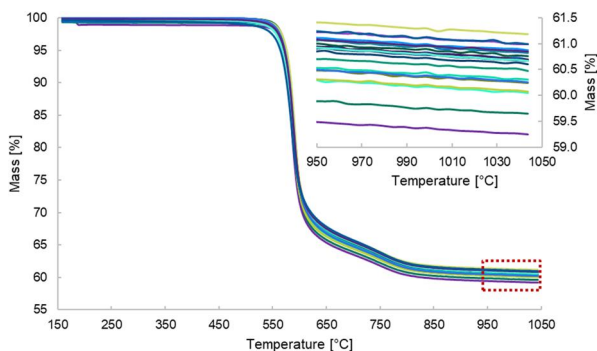


Figure 15. TGA curves of all samples up to 1050 °C in nitrogen atmosphere, showing the carbon yield as a function of annealing temperature and time.

leading to a more stable polymer structure, as proven by the resistance against concentrated sulfuric acid.

An exact quantification of dissolution, however, was not possible due to the mixture of fiber sticks and the gel parts.

3.6. Shape stability by optical verification

The optical stability test confirmed the previous analytic results. The deformation of the parts and

therefore the measured height decreased with annealing temperature and time due to the higher degree of crosslinking. Hence, the shape stability increased tremendously. In Figure 16, the cone-shaped specimens are displayed. Figure 16(a) shows the parts after the thermal annealing step. In terms of the shape, there were no obvious differences between the parts. The changes of the shape stability are summarized in Figure 16(b) after a melting test at 450 °C for one hour. The as-printed sample visibly remelted. The 6 h samples also revealed some geometric deformations.

In order to quantify the optical impressions of the shape changes, the heights of the cones were measured before and after the 450 °C step. The shrinkage and remelt characteristics of the parts are shown in Figure 17.

To account for minor variations in sample height, percentage shrinkage measurements before and after thermal annealing instead of absolute shrinkage were used. The optical impressions were confirmed by quantified measurements. The height shrinkage of the samples annealed at low temperatures and short times revealed a shrinkage of about 8%, whereas the samples annealed at temperatures near the melting point and times ≥ 24 h showed almost no shrinkage. Regarding the tool-free and near net shape processing, the geometrical stabilization is crucial.

4. Conclusion

In order to use additive manufacturing for the CFRP fabrication and PEEK as precursor for ceramic matrix composites, the study focused on the shape

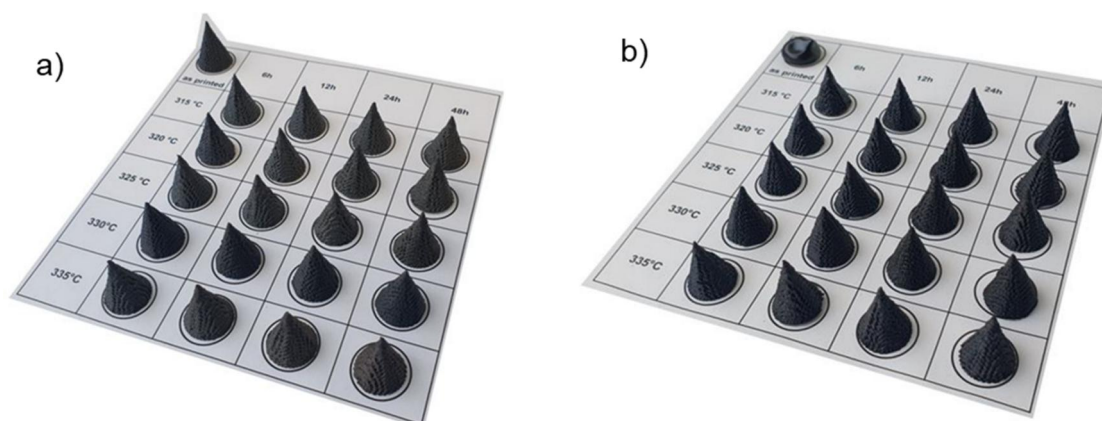


Figure 16. Images of the CF-PEEK cone parts (a) after the annealing and (b) after the melting test at 450 °C for one hour.

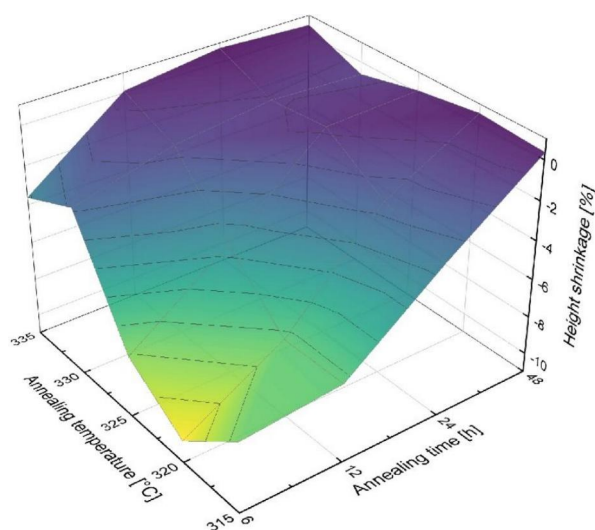


Figure 17. Height shrinkage as a function of annealing time and temperature after heat treatment at 450 °C for one hour.

stabilization of the thermally induced crosslinking process of CF-PEEK below its melting temperature. The analytic measurements confirmed a rising influence on the stabilization of the CF-PEEK as a function of increasing annealing temperatures and times below the melting point of PEEK. The DSC results revealed an increasing T_g as well as decreasing melting enthalpy and a shift to lower melting points for increasing annealing temperatures and times. The rheological analysis confirmed that results by increasing storage modules and decreasing loss modules with increasing annealing time and temperature. In previous studies, similar effects are often described as competing effects consisting of chain branching, scission and crosslinking. These competing mechanisms occurring at certain temperatures were in good agreement with this study. Furthermore, the kinetic analysis indicated a thermally induced crosslinking process. Within the limitations given by the thermal requirements, the investigated annealing temperatures varied from 315 °C to 335 °C, while the annealing

times were set from 6 h to 48 h. The main conclusions of this study are therefore:

- The shape stabilization increases with annealing temperature and annealing time.
- The thermally induced crosslinking can be well described by a kinetic model with high accuracy of $R^2 = 0.99$.
- The initiating conditions for the crosslinking of CF-PEEK should exceed a certain temperature of at least >315 °C in combination with a sufficient annealing time of at least ≥ 12 hours.

In view of rising costs for the post treatment and saving resources due to less produced waste and an increased sustainability, this technology has high potential. Controlling the process can highly impact the manufacturing of CMC parts in the future. Especially the near net shape fabrication of complex geometries opens new fields of applications.

Disclosure statement

No potential competing interest was reported by the authors.

Funding

This work was supported by the DFG (German Research Foundation) grant number LA 4649/1-1.

ORCID

Wolfgang Freudenberg  <http://orcid.org/0000-0001-6157-0726>

Data availability statement

The data that support the findings of this study are available from the corresponding author, (Wolfgang Freudenberg), upon reasonable request.

References

- Chawla KK. Ceramic matrix composites. Boston, MA, s.l Springer US; 1993.
- Lenoe EM, Katz RN, Burke JJ, editors. Ceramics for high-performance applications III - Reliability: Proceedings of the Sixth Army Materials Technology Conference, held July 10 - 13, 1979, at Orcas Island, Washington; Army Materials Technology Conference series, 6. New York: Plenum Press; 1983.
- Bansal NP, editor. Handbook of ceramic composites. 1st ed. New York (NY): Springer US; 2005; Imprint: Springer.
- Krenkel W. Ceramic matrix composites: fiber reinforced ceramics and their applications. Weinheim: Wiley-VCH; 2008.
- Kumar S, Shekar KC, Jana B, et al. C/C and C/SiC composites for aerospace applications. In: Prasad NE, Wanhill, RJH, editors. Aerospace Materials. Singapore: Springer;2017:343–369.
- Padture NP. Advanced structural ceramics in aerospace propulsion. *Nat Mater.* 2016;15(8):804–809. doi: [10.1038/nmat4687](https://doi.org/10.1038/nmat4687).
- Tang S, Hu C. Design, preparation and properties of carbon fiber reinforced ultra-high temperature ceramic composites for aerospace applications: a review. *J Mater Sci Technol.* 2017;33(2):117–130. doi: [10.1016/j.jmst.2016.08.004](https://doi.org/10.1016/j.jmst.2016.08.004).
- Huang X. Fabrication and properties of carbon fibers. *Materials.* 2009;2(4):2369–2403. doi: [10.3390/ma2042369](https://doi.org/10.3390/ma2042369).
- MInus M, Kumar S. The processing, properties, and structure of carbon fibers. *JOM.* 2005;57(2):52–58. doi: [10.1007/s11837-005-0217-8](https://doi.org/10.1007/s11837-005-0217-8).
- Chen Z, Li Z, Li J, et al. 3D printing of ceramics: a review. *J Eur Ceram Soc.* 2019;39(4):661–687. doi: [10.1016/j.jeurceramsoc.2018.11.013](https://doi.org/10.1016/j.jeurceramsoc.2018.11.013).
- Li W, Armani A, Martin A, et al. Extrusion-based additive manufacturing of functionally graded ceramics. *J Eur Ceram Soc.* 2021;41(3):2049–2057. doi: [10.1016/j.jeurceramsoc.2020.10.029](https://doi.org/10.1016/j.jeurceramsoc.2020.10.029).
- Li Q, Zhao W, Niu B, et al. 3D printing high interfacial bonding polyether ether ketone components via pyrolysis reactions. *Mater Design.* 2021;198:109333. doi: [10.1016/j.matdes.2020.109333](https://doi.org/10.1016/j.matdes.2020.109333).
- van de Werken N, Koirala P, Ghorbani J, et al. Investigating the hot isostatic pressing of an additively manufactured continuous carbon fiber reinforced PEEK composite. *Addit Manuf.* 2021;37:101634. doi: [10.1016/j.addma.2020.101634](https://doi.org/10.1016/j.addma.2020.101634).
- Wang W, Zhang L, Dong X, et al. Additive manufacturing of fiber reinforced ceramic matrix composites: advances, challenges, and prospects. *Ceram Int.* 2022;48(14):19542–19556. doi: [10.1016/j.ceramint.2022.04.146](https://doi.org/10.1016/j.ceramint.2022.04.146).
- Flauder S, Langhof N, Krenkel W, et al. Size effect of carbon fiber-reinforced silicon carbide composites (C/C-SiC): part 1 – bending load and statistical effects. *J Eur Ceram Soc.* 2021;41(14):6805–6814. doi: [10.1016/j.jeurceramsoc.2021.07.040](https://doi.org/10.1016/j.jeurceramsoc.2021.07.040).
- van de Werken N, Tekinalp H, Khanbolouki P, et al. Additively manufactured carbon fiber-reinforced composites: state of the art and perspective. *Addit Manuf.* 2020;31:100962. doi: [10.1016/j.addma.2019.100962](https://doi.org/10.1016/j.addma.2019.100962).
- Chacón JM, Caminero MA, Núñez PJ, et al. Additive manufacturing of continuous fibre reinforced thermoplastic composites using fused deposition modelling: effect of process parameters on mechanical properties. *Compos Sci Technol.* 2019;181:107688. doi: [10.1016/j.compscitech.2019.107688](https://doi.org/10.1016/j.compscitech.2019.107688).
- Liu G, Xiong Y, Zhou L. Additive manufacturing of continuous fiber reinforced polymer composites: design opportunities and novel applications. *Compos Commun.* 2021;27:100907. doi: [10.1016/j.coco.2021.100907](https://doi.org/10.1016/j.coco.2021.100907).
- Ning F, Cong W, Qiu J, et al. Additive manufacturing of carbon fiber reinforced thermoplastic composites using fused deposition modeling. *Compos Part B: Eng.* 2015;80:369–378. doi: [10.1016/j.compositesb.2015.06.013](https://doi.org/10.1016/j.compositesb.2015.06.013).
- Pascual-González C, San Martín P, Lizarralde I, et al. Post-processing effects on microstructure, interlaminar and thermal properties of 3D printed continuous carbon fibre composites. *Compos Part B: Eng.* 2021;210:108652. doi: [10.1016/j.compositesb.2021.108652](https://doi.org/10.1016/j.compositesb.2021.108652).
- Penumakala PK, Santo J, Thomas A. A critical review on the fused deposition modeling of thermoplastic polymer composites. *Compos Part B: Eng.* 2020;201:108336. doi: [10.1016/j.compositesb.2020.108336](https://doi.org/10.1016/j.compositesb.2020.108336).
- Wong J, Altassan A, Rosen DW. Additive manufacturing of fiber-reinforced polymer composites: a technical review and status of design methodologies. *Compos Part B: Eng.* 2023;255:110603. doi: [10.1016/j.compositesb.2023.110603](https://doi.org/10.1016/j.compositesb.2023.110603).
- Yuan S, Li S, Zhu J, et al. Additive manufacturing of polymeric composites from material processing to structural design. *Compos Part B: Eng.* 2021;219:108903. doi: [10.1016/j.compositesb.2021.108903](https://doi.org/10.1016/j.compositesb.2021.108903).
- Zhuo P, Li S, Ashcroft IA, et al. Material extrusion additive manufacturing of continuous fibre reinforced polymer matrix composites: a review and outlook. *Compos Part B: Eng.* 2021;224:109143. doi: [10.1016/j.compositesb.2021.109143](https://doi.org/10.1016/j.compositesb.2021.109143).
- Wich F, Flauder S, Schneider N, et al. Processing properties and pyrolysis behavior of novolak-hexamethylenetetramine mixtures. *Adv Manuf: Polym Compos Sci.* 2023;9(1):2187687. doi: [10.1080/20550340.2023.2187687](https://doi.org/10.1080/20550340.2023.2187687).
- Reichert F, Langhof N, Krenkel W. The evaluation of thermoplastic precursors for C/C-SiC manufactured by liquid silicon infiltration (LSI). *MSF.* 2015;825-826:232–239. doi: [10.4028/www.scientific.net/MSF.825-826.232](https://doi.org/10.4028/www.scientific.net/MSF.825-826.232).
- Reichert F, Pérez-Mas AM, Barreda D, et al. Influence of the carbonization temperature on the mechanical properties of thermoplastic polymer derived C/C-SiC composites. *J Eur Ceram Soc.* 2017;37(2):523–529. doi: [10.1016/j.jeurceramsoc.2016.09.005](https://doi.org/10.1016/j.jeurceramsoc.2016.09.005).
- Flauder S, Bombarda I, D'Ambrosio R, et al. Size effect of carbon fiber-reinforced silicon carbide composites (C/C-SiC): part 2 - tensile testing with alignment device. *J Eur Ceram Soc.* 2022;42(4):1227–1237. doi: [10.1016/j.jeurceramsoc.2021.11.044](https://doi.org/10.1016/j.jeurceramsoc.2021.11.044).
- Liensdorf T, Langhof N, Krenkel W. Mechanical properties of PEEK-derived C/SiC composites with

- different fiber lengths. *Adv Eng Mater.* 2019;21(5):1800835. doi: [10.1002/adem.201800835](https://doi.org/10.1002/adem.201800835).
30. Freudenberg W, Wich F, Langhof N, et al. Additive manufacturing of carbon fiber reinforced ceramic matrix composites based on fused filament fabrication. *J Eur Ceram Soc.* 2022;42(4):1822–1828. doi: [10.1016/j.jeurceramsoc.2021.12.005](https://doi.org/10.1016/j.jeurceramsoc.2021.12.005).
31. Bianchi G, Vodermayr A, Ortona A. Net shape CMC components produced by composite flow moulding, pyrolysis and reactive silicon infiltration. *Ceram Int.* 2018;44(11):12204–12209. doi: [10.1016/j.ceramint.2018.03.279](https://doi.org/10.1016/j.ceramint.2018.03.279).
32. Best J, Freudenberg W, Langhof N, et al. Processing-microstructure correlations in material extrusion additive manufacturing of carbon fiber reinforced ceramic matrix composites. *Addit Manuf.* 2024;79:103888. doi: [10.1016/j.addma.2023.103888](https://doi.org/10.1016/j.addma.2023.103888).
33. Cuan-Urquiza E, Barocio E, Tejada-Ortigoza V, et al. Characterization of the mechanical properties of FFF structures and materials: a review on the experimental, computational and theoretical approaches. *Materials.* 2019;12(6):895. doi: [10.3390/ma12060895](https://doi.org/10.3390/ma12060895).
34. Patel P, Hull TR, McCabe RW, et al. Mechanism of thermal decomposition of poly(ether ether ketone) (PEEK) from a review of decomposition studies. *Polym Degrad Stab.* 2010;95:709–718. doi: [10.1016/j.polymdegradstab.2010.01.024](https://doi.org/10.1016/j.polymdegradstab.2010.01.024).
35. Ramgobin A, Fontaine G, Bourbigot S. A case study of polyether ether ketone (I): investigating the thermal and fire behavior of a high-performance material. *Polymers.* 2020;12(8):1789. doi: [10.3390/polym12081789](https://doi.org/10.3390/polym12081789).
36. Patel P, Hull TR, Lyon RE, et al. Investigation of the thermal decomposition and flammability of PEEK and its carbon and glass-fibre composites. *Polym Degrad Stab.* 2011;96(1):12–22. doi: [10.1016/j.polymdegradstab.2010.11.009](https://doi.org/10.1016/j.polymdegradstab.2010.11.009).
37. Shabaev AS, Zhansitov AA, Khakymasheva EV, et al. Study of thermo-oxidative transformations of unstabilized and stabilized poly(ether ether ketone). *Polym Sci Ser B.* 2019;61(5):582–588. doi: [10.1134/S1560090419050154](https://doi.org/10.1134/S1560090419050154).
38. Barış Vatandaş B, Uşun A, Yıldız N, et al. Additive manufacturing of PEEK-based continuous fiber reinforced thermoplastic composites with high mechanical properties. *Compos Part A: Appl Sci Manuf.* 2023;167:107434. doi: [10.1016/j.compositesa.2023.107434](https://doi.org/10.1016/j.compositesa.2023.107434).
39. Diouf-Lewis A, Farahani RD, Iervolino F, et al. Design and characterization of carbon fiber-reinforced PEEK/PEI blends for Fused Filament Fabrication additive manufacturing. *Mater Today Commun.* 2022;31:103445. doi: [10.1016/j.mtcomm.2022.103445](https://doi.org/10.1016/j.mtcomm.2022.103445).
40. Lee A, Wynn M, Quigley L, et al. Effect of temperature history during additive manufacturing on crystalline morphology of PEEK. *Adv Ind Manuf Eng.* 2022;4:100085. doi: [10.1016/j.aime.2022.100085](https://doi.org/10.1016/j.aime.2022.100085).
41. Su Y, He J, Jiang N, et al. Additively-manufactured poly-ether-ether-ketone (PEEK) lattice scaffolds with uniform microporous architectures for enhanced cellular response and soft tissue adhesion. *Mater Design.* 2020;191:108671. doi: [10.1016/j.matdes.2020.108671](https://doi.org/10.1016/j.matdes.2020.108671).
42. Wang Y, Müller W-D, Rumjahn A, et al. Mechanical properties of fused filament fabricated PEEK for biomedical applications depending on additive manufacturing parameters. *J Mech Behav Biomed Mater.* 2021;115:104250. doi: [10.1016/j.jmbbm.2020.104250](https://doi.org/10.1016/j.jmbbm.2020.104250).
43. Zheng J, Zhao H, Dong E, et al. Additively-manufactured PEEK/HA porous scaffolds with highly-controllable mechanical properties and excellent biocompatibility. *Mater Sci Eng C Mater Biol Appl.* 2021;128:112333. doi: [10.1016/j.msec.2021.112333](https://doi.org/10.1016/j.msec.2021.112333).
44. Zheng J, Zhao H, Ouyang Z, et al. Additively-manufactured PEEK/HA porous scaffolds with excellent osteogenesis for bone tissue repairing. *Compos Part B: Eng.* 2022;232:109508. doi: [10.1016/j.compositesb.2021.109508](https://doi.org/10.1016/j.compositesb.2021.109508).
45. Al Lafi AG, Parker DJ, Hay JN. The crosslinking of poly(ether ether ketone): thermally and by irradiation. *J Appl Polym Sci.* 2015;132(22). doi: [10.1002/app.41999](https://doi.org/10.1002/app.41999).
46. Pascual A, Toma M, Tsotra P, et al. On the stability of PEEK for short processing cycles at high temperatures and oxygen-containing atmosphere. *Polym Degrad Stab.* 2019;165:161–169. doi: [10.1016/j.polydegradstab.2019.04.025](https://doi.org/10.1016/j.polydegradstab.2019.04.025).
47. Bayerl T, Brzeski M, Martínez-Tafalla M, et al. Thermal degradation analysis of short-time heated polymers. *J Thermoplast Compos Mater.* 2015;28(3):390–414. doi: [10.1177/0892705713486122](https://doi.org/10.1177/0892705713486122).
48. Phillips R, Glauser T, Månson J-AE. Thermal stability of PEEK/carbon fiber in air and its influence on consolidation. *Polym Compos.* 1997;18(4):500–508. doi: [10.1002/pc.10302](https://doi.org/10.1002/pc.10302).
49. Day M, Sally D, Wiles DM. Thermal degradation of poly(aryl-ether-ether-ketone): experimental evaluation of crosslinking reactions. *J Appl Polym Sci.* 1990;40(910):1615–1625. doi: [10.1002/app.1990.070400917](https://doi.org/10.1002/app.1990.070400917).
50. Day M, Suprunchuk T, Cooney JD, et al. Thermal degradation of poly(aryl-ether-ether-ketone) (PEEK): a differential scanning calorimetry study. *J Appl Polym Sci.* 1988;36(5):1097–1106. doi: [10.1002/app.1988.070360510](https://doi.org/10.1002/app.1988.070360510).
51. Tsotra P, Toma M, Pascual A, et al. Dransfeld: 'ECCM17_Paper_Template'. ECCM18 - 18th European Conference on Composite Materials Athens, Greece, 24–28th June 2018.
52. Ehrenstein GW, Riedel G, Trawiel P. *Thermal analysis of plastics: theory and practice.* München: Hanser Verlag; 2004.
53. Jonas A, Legras R. Thermal stability and crystallization of poly(aryl ether ether ketone). *Polymer.* 1991;32(15):2691–2706. doi: [10.1016/0032-3861\(91\)90095-Z](https://doi.org/10.1016/0032-3861(91)90095-Z).
54. McLauchlin AR, Ghita OR, Savage L. Studies on the reprocessability of poly(ether ether ketone) (PEEK). *J Mater Process Technol.* 2014;214:75–80. doi: [10.1016/j.jmatprotec.2013.07.010](https://doi.org/10.1016/j.jmatprotec.2013.07.010).
55. Cole KC, Casella IG. Fourier transform infrared spectroscopic study of thermal degradation in films of poly(etheretherketone). *Thermochim*

- Acta. 1992;211:209–228. doi: [10.1016/0040-6031\(92\)87021-2](https://doi.org/10.1016/0040-6031(92)87021-2).
56. Courvoisier E, Bicaba Y, Colin X. Multi-scale and multi-technique analysis of the thermal degradation of poly(ether ether ketone). *Polym Degrad Stab*. 2018;151:65–79. doi: [10.1016/j.polymdegradstab.2018.03.001](https://doi.org/10.1016/j.polymdegradstab.2018.03.001).
 57. Zhiyi Z ,Zeng H. Effects of thermal treatment on poly(-ether ehter ketone). *Polymer*. 1993;34(17):3648–3652. doi: [https://doi.org/10.1016/0032-3861\(93\)90049-G](https://doi.org/10.1016/0032-3861(93)90049-G).
 58. Cebe P. Annealing study of poly(etheretherketone). *J Mater Sci*. 1988;23(10):3721–3731. doi: [10.1007/BF00540520](https://doi.org/10.1007/BF00540520).
 59. Cebe P, Hong S-D. Crystallization behaviour of poly(ether-ether-ketone). *Polymer*. 1986;27(8):1183–1192. doi: [10.1016/0032-3861\(86\)90006-6](https://doi.org/10.1016/0032-3861(86)90006-6).
 60. de Almeida O, Feuillerat L, Fontanier J-C, et al. Determination of a degradation-induced limit for the consolidation of CF/PEEK composites using a thermo-kinetic viscosity model. *Compos Part A Appl Sci Manuf*. 2022;158:106943. doi: [10.1016/j.compositesa.2022.106943](https://doi.org/10.1016/j.compositesa.2022.106943).
 61. Vyazovkin S, Burnham AK, Favregeon L, et al. ICTAC Kinetics Committee recommendations for analysis of multi-step kinetics. *Thermochim Acta*. 2020;689:178597. doi: [10.1016/j.tca.2020.178597](https://doi.org/10.1016/j.tca.2020.178597).